

# Perfect Andreev Reflection of Helical Edge Modes in Inverted InAs/GaSb Quantum Wells

Ivan Knez and Rui-Rui Du

*Department of Physics and Astronomy, Rice University, Houston, TX 77251-1892*

Gerard Sullivan

*Teledyne Scientific and Imaging, Thousand Oaks, CA 91630*

Quantum Spin Hall Insulator (QSHI) is a two-dimensional variant of a novel class of materials characterized by topological order, whose unique properties have recently triggered much interest and excitement in the condensed matter community.<sup>1,2</sup> Most notably, topological properties of these systems hold great promise in mitigating the difficult problem of decoherence in implementations of quantum computers.<sup>3</sup> Although QSHI has been theoretically predicted in a few different materials,<sup>4-7</sup> so far only the semiconductor systems of HgTe/CdTe<sup>8</sup> and, more recently, inverted InAs/GaSb,<sup>9</sup> have shown direct evidence for the existence of this phase. Ideally insulating in the bulk, QSHI is characterized by one-dimensional channels at the sample perimeter, which have helical property, with carrier spin tied to the carrier direction of motion, and protected from back-scattering by time-reversal symmetry. Here we experimentally show that QSH edge channels in InAs/GaSb exhibit perfect Andreev reflection (AR), validating their helical property and topological protection from back-scattering.

Much of the transport phenomenology of QSHI has been established in a set of remarkable experiments in HgTe material system,<sup>8,10</sup> including the quantized conductance and the non-local character of the QSH edge modes. Combining QSHI with superconductors is the next experimental challenge, posing fundamental questions regarding the nature of topological superconductors and the possible realizations of Majorana fermion excitations.<sup>3,11-13</sup> Recently it has been theoretically suggested that Andreev reflection can be used as a powerful method to probe helical edge modes.<sup>14</sup> InAs/GaSb material system is well suited for the task, due to its low Schottky barrier and good interface to superconductors.<sup>15-17</sup>

In this Letter, we study inverted InAs/GaSb quantum wells (QWs) contacted by superconducting electrodes. We observe strong zero-bias dips in the differential resistance as the Fermi level is tuned across the hybridization gap via a front gate. Analysis of the relative size of the dips and corresponding gap excess current is in agreement with expectations of perfect Andreev reflection of the helical edge modes. The perfect AR occurs in spite of a finite barrier at the interface, with the interface transmissivity estimated to  $T = 0.7$ . Excess current and differential resistance dips show only a weak temper-

ature dependence for temperatures lower than the critical temperature of the superconducting electrodes. On the other hand, weak magnetic fields of less than 50 mT are sufficient to completely suppress excess current in the hybridization gap, indicating strong sensitivity to time-reversal breaking.

InAs/GaSb QWs contain both electron and hole two-dimensional gases situated in InAs and GaSb layers respectively, and enclosed with AlSb barriers. Sample structure is shown in Fig. 1 inset a. In the inverted regime, the electron subband is lower than the hole subband leading to band anti-crossing and mini-gap opening.<sup>18-20</sup> Energy spectrum with the resulting hybridization gap is shown in Fig. 1 inset b. Due to the band inversion, helical edge modes appear in the mini gap.<sup>7,9</sup> In order to probe the helical character of the edge modes, superconducting niobium electrodes with critical temperature of  $T_c = 8.27$  K (BCS gap of  $\Delta_S = 1.24$  meV) are deposited directly on the InAs layers, while the electrostatic front gate is used to tune the Fermi energy  $E_F$  into the hybridization regime.

Andreev reflection<sup>21</sup> is a process unique to the superconductor-normal metal (S-N) interface, where impinging normal quasiparticle retroreflects, having thus not only opposite velocity but also opposite charge, and resulting in the enhancement of the total current across the interface. The electrical current through a single S-N interface can be calculated using the Blonder-Tinkham-Klapwijk (BTK) model:<sup>22</sup>

$$I = \frac{N \cdot e}{h} \int [f(E + eV) - f(E)][1 + A(E) - B(E)] dE \quad (1)$$

where  $N$  is the number of modes in the normal conductor,  $f(E)$  is the equilibrium Fermi distribution function,  $V$  is the voltage drop at the interface, and  $A(E)$  and  $B(E)$  are probabilities for Andreev and normal reflection (NR) of the electron at the interface. In the case of ideal interface, and for biases within the superconducting gap ( $V < \frac{\Delta_S}{e}$ ), quasi-particles are only Andreev reflected. This is because within the superconducting gap transmission is prohibited, and there is no potential barrier which would absorb the momentum difference necessary for normal reflection. In practice, due to native oxides or Schottky barriers, a potential step always exists at the S-N interface, allowing for normal reflection and hence reducing the probability for Andreev reflection. The interface barrier is characterized by the scat-

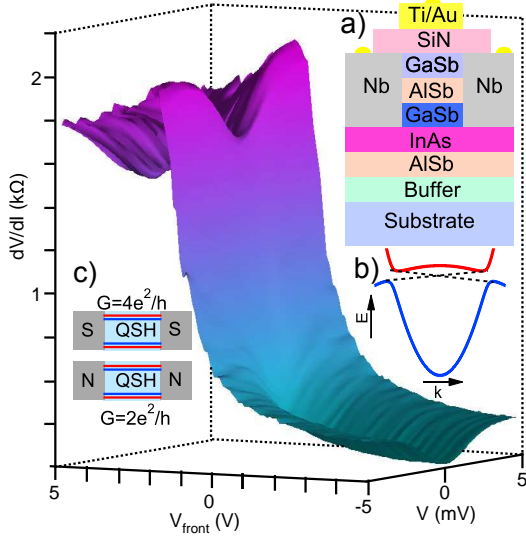


Figure 1: **Transport in S-QSH-S junctions.** Figure shows differential resistance  $dV/dI$  vs bias voltage  $V$  across the S-InAs/GaSb-S junction and vs front gate bias  $V_{front}$ . Inset **a** shows device cross-section while inset **b** shows energy spectrum of inverted InAs/GaSb QWs with linearly dispersing helical edge modes in the mini-gap. As the Fermi level  $E_F$  is tuned across the mini-gap via  $V_{front}$ ,  $dV/dI$  exhibits strong peak at larger  $V$ . On the other hand, for  $V$  close to zero,  $dV/dI$  exhibits strong dips, suggesting transport dominated by Andreev reflection processes. Inset **c** shows two-terminal structure with superconducting and normal leads. Due to the perfect Andreev reflection at S-QSH interfaces, voltage drop at each contact is halved, leading to doubling of differential conductance compared to N-QSH case.

tering parameter  $Z$  which is related to the normal transmission of the barrier as  $T = \frac{1}{1+Z^2}$ . For  $Z < 1$ , AR dominates over NR resulting in zero bias dips in differential resistance  $dV/dI$ . In this case, current enhancement due to AR also manifests itself as an excess current  $I_{excess}$ , which is obtained by extrapolating linear  $I - V$  curve at high biases, i.e. for  $V \gg \frac{\Delta_S}{e}$ , to zero bias.

Fig. 1 shows  $dV/dI$  vs bias voltage  $V$  across the S-InAs/GaSb-S junction and front gate bias  $V_{front}$ . As  $E_F$  is tuned into the mini-gap via  $V_{front}$ ,  $dV/dI$  exhibits strong peak at larger biases ( $V \gg \frac{\Delta_S}{e}$ ). On the other hand, for  $V < \frac{2\Delta_S}{e}$ ,  $dV/dI$  exhibits strong dips, i.e. enhanced conduction due to AR. Fig. 2a shows normal resistance  $R_N$ , i.e.  $dV/dI$  for  $V \gg \frac{\Delta_S}{e}$ , vs  $V_{front}$  (in blue) and  $I_{excess}$  vs.  $V_{front}$  (in red). As  $E_F$  is tuned towards the mini-gap,  $R_N$  increases towards the peak value of  $\sim 2 \text{ k}\Omega$  signaling mini-gap entry, while concurrently  $I_{excess}$  decreases from the maximal value of  $\sim 2.6 \mu\text{A}$  to the mini-gap value of  $I_{excess} \sim 150 \text{ nA}$ . In Fig. 2b we plot  $I - V$  and  $dV/dI - V$  curves for  $V_{front} = 5 \text{ V}$ . In this case  $E_F$  is high above the hybridization gap. Strong zero-bias dips in  $dV/dI - V$  curve are observed, while  $I - V$  shows evident non-linear character. Extrapolat-

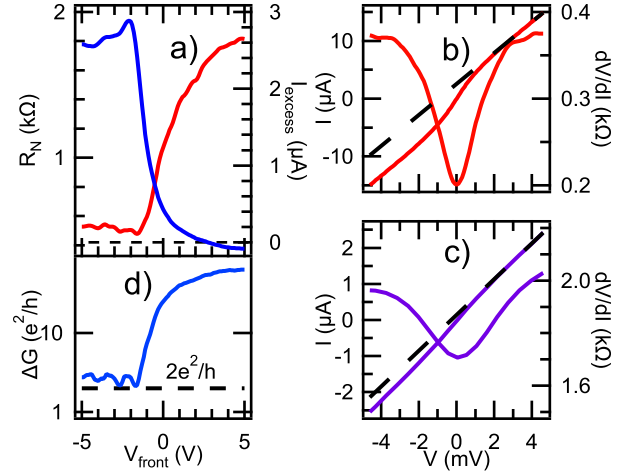


Figure 2: **Perfect Andreev reflection of helical edges.** Panel **a** shows normal resistance  $R_N$  (in blue) and excess current due to Andreev reflection  $I_{excess}$  (in red) vs  $V_{front}$ . As  $V_{front}$  is decreased,  $E_F$  is tuned towards the mini-gap and  $R_N$  increases towards the peak value of  $\sim 2 \text{ k}\Omega$ , while concurrently  $I_{excess}$  decreases from the maximal value of  $\sim 2.6 \mu\text{A}$  ( $V_{front} = 5 \text{ V}$ ) to mini-gap value  $I_{excess} \sim 150 \text{ nA}$  ( $V_{front} = -2.1 \text{ V}$ ). Panel **b** and **c** show  $dV/dI$  and  $I$  vs  $V$  for  $V_{front} = 5 \text{ V}$  and  $V_{front} = -2.1 \text{ V}$  respectively. Excess current is determined as an intercept of the linear fit to the  $I - V$  curve for large  $V$ . Panel **d** shows conductance difference  $\Delta G \equiv G(V=0) - G(V \gg \Delta_S/e)$  vs  $V_{front}$  on a log scale. For  $E_F$  in the mini-gap  $\Delta G$  plateaus at  $2e^2/h$ , indicating perfect AR of helical edge channels.

ing current from high biases gives  $I_{excess} \sim 2.6 \mu\text{A}$ . The scattering parameter of the barrier can be estimated from the ratio  $\frac{e \cdot I_{excess} \cdot R_N}{\Delta_S} \sim 0.76$ , to give  $Z = 0.65$  and normal transmissivity of  $T = 0.7$ .<sup>23,24</sup> This transmissivity is only slightly lower than the largest reported value of 0.86 for the InAs material system.<sup>17</sup> In spite of high barrier transmissivity, the absence of supercurrent in our structures suggests that coherence is not preserved across the junction, presumably due to the surface degradation during plasma cleaning. Nevertheless, this simplifies the analysis in the case when  $E_F$  is in the mini-gap, allowing us to add conductance contributions from each S-QSH interface independently, as previously done in N-QSH-N structures.<sup>8,9</sup>

In the case of S-QSH single edge interface, the absence of back-scattering channels in the helical edge requires NR probability  $B(E) = 0$  at all energies. Within the superconducting gap ( $E < \Delta_S$ ), electron transmission is excluded, requiring a perfect AR with probability  $A(E) = 1$ .<sup>14</sup> Evaluating equation (1) in zero temperature limit for this case gives a contact resistance for a single helical edge channel of  $\frac{h}{4e^2}$  when  $V < \frac{\Delta_S}{e}$ . In two-terminal geometry, used in our experiments, this gives a resistance of each helical edge mode to be  $\frac{h}{4e^2} + \frac{h}{4e^2} = \frac{h}{2e^2}$ , giving a total two-terminal resistance of  $\frac{h}{2e^2} \parallel \frac{h}{2e^2} = \frac{h}{4e^2}$ . On the other hand, for  $V \gg \frac{\Delta_S}{e}$ , electron transmission

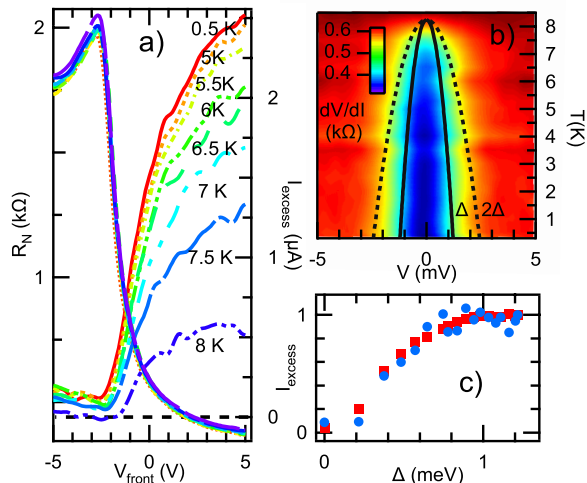


Figure 3: **Temperature dependence.** Panel **a** shows  $R_N$  and  $I_{excess}$  vs  $V_{front}$  for temperature  $T=0.5$  K, and  $T$  from 5 K to 8 K varied in 0.5 K increments. Dependence is exceptionally weak except when  $T$  approaches  $T_c = 8.27$  K. Panel **b** shows color map of  $dV/dI$  vs  $V$  and  $T$  ( $V_{front} = 0$  V). Full and dashed lines show BCS dependence of the superconducting gap  $\Delta_S/e$  and  $2\Delta_S/e$  respectively. Dips in  $dV/dI$  follow closely the BCS gap  $\Delta_S$ . Panel **c** shows normalized  $I_{excess}$ , i.e.  $I_{excess}(T)/I_{excess}(300\text{ mK})$ , vs  $\Delta_S(T)$  for  $E_F$  above the mini-gap (in red) and  $E_F$  in the mini-gap (in blue). In both cases, normalized  $I_{excess}$  shows equal decrease as the  $\Delta_S$  is reduced with  $T$ .

into the superconducting lead becomes possible and AR probability scales to zero as  $A(E) \sim (\frac{\Delta_S}{E})^2 \rightarrow 0$ ,<sup>22</sup> reducing equation (1) to the familiar case of N-QSH interface with a contact resistance of  $\frac{h}{2e^2}$ . Simple resistance combination now gives a total two-terminal resistance of  $\frac{h}{2e^2}$ .

In InAs/GaSb QWs this analysis may be further complicated by the presence of low mobility mini-gap bulk carriers.<sup>20,25</sup> However, we note here that scattered states, which lead to residual bulk conductivity due to their loss of quantum properties and inability to tunnel,<sup>20,25,26</sup> are not expected to participate in AR which is a quantum process. As a result, difference between two-terminal conductances at zero and high biases will be:  $\Delta G \equiv G(V=0) - G(V \gg \Delta_S/e) = \frac{2e^2}{h}$  (Fig. 1 inset c). Note that in Fig. 2c, where  $E_F$  is in the hybridization gap,  $\frac{dV}{dT}(V=0) \sim 1.7\text{ k}\Omega$ , while  $\frac{dV}{dT}(V \gg \Delta_S/e) \sim 2\text{ k}\Omega$ . Inverting these two values gives  $\Delta G \sim 2.2\frac{e^2}{h}$ , which is surprisingly close to the expected value of  $\frac{2e^2}{h}$ . This is better illustrated in Fig. 2d, which shows plateauing of  $\Delta G$  to a conductance value of  $\frac{2e^2}{h}$ , as  $E_F$  is pushed into the hybridization gap, validating the picture of perfect AR of helical edge channels.

Furthermore, dissimilar conductance values within and outside of the superconductive gap translate into non-linear  $I - V$  curve which can be approximated by  $I =$

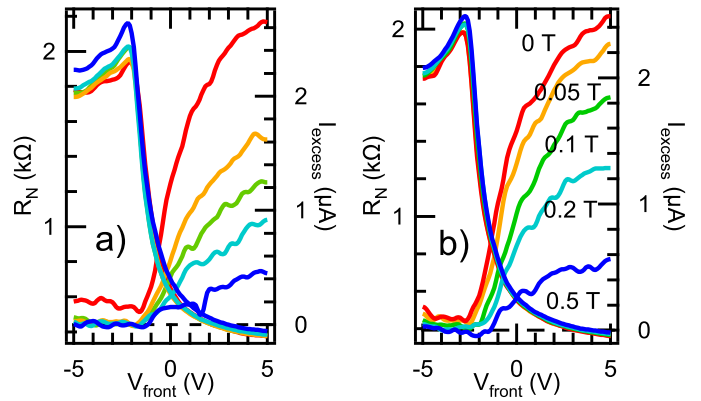


Figure 4: **Magnetic field dependence.** Panels show  $R_N$  and  $I_{excess}$  vs  $V_{front}$  for perpendicular magnetic fields of  $B_{\perp} = 0$  T, 0.05 T, 0.1 T, 0.2 T, and 0.5 T in **a** and in **b** for in-plane magnetic fields  $B_{\parallel}$  with the same increments. Although for  $E_F$  above the hybridization gap,  $I_{excess}$  survives up to 0.5 T, for  $E_F$  in the mini-gap  $I_{excess}$  is completely suppressed with  $B_{\perp} = 0.05$  T and  $B_{\parallel} = 0.1$  T. This is in contrast to the equal suppression of  $I_{excess}$  in temperature dependence (Fig. 3c), suggesting different nature of excess current in and outside of the hybridization gap.

$\left(\frac{4e^2}{h} + G_{bulk}\right)V$  for  $V < \frac{\Delta_S}{e}$  and  $I = \left(\frac{2e^2}{h} + G_{bulk}\right)V + \frac{2e\Delta_S}{h}$  for  $V > \frac{\Delta_S}{e}$ . The intercept of the latter equation gives an estimate of the excess current as  $I_{excess} \sim \frac{2e\Delta_S}{h} \sim 100\text{ nA}$ . Considering the approximative character of the given analysis, the latter value is in reasonable agreement with the measured value of 150 nA in Fig. 2a and 2c.

The temperature dependence of  $I_{excess}$  in Fig. 3a shows only a weak dependence for temperatures up to 6.5 K and it is quickly suppressed as the temperature is further increased towards the critical temperature of niobium leads. Furthermore, a color map of temperature evolution of  $dV/dI$  is shown in Fig. 3b, with dips in  $dV/dI$  closely following the BCS temperature dependence of superconducting gap  $\Delta_S$ . We note here that  $I_{excess}$  for  $E_F$ , both inside and outside of the mini-gap, show comparative suppression when  $\Delta_S$  is reduced with increased temperature. This is most easily seen when  $I_{excess}$  is normalized by the corresponding low temperature values, i.e.  $I_{excess}(T)/I_{excess}(300\text{ mK})$  and plotted in Fig. 3c for these two cases.

This is in sharp contrast to the magnetic field dependence of  $I_{excess}$  shown in Fig. 4, where  $I_{excess}$  for  $E_F$  in the mini-gap is suppressed much faster than in the case when  $E_F$  is outside of the mini-gap. In fact, perpendicular magnetic fields of less than 50 mT are sufficient to fully suppress AR processes in the mini-gap, while above the mini-gap AR processes survive in fields up to at least 500 mT. Similar disproportionality is also observed for the in-plane magnetic fields, albeit in this case mini-gap  $I_{excess}$  survives for fields up to 100 mT while above the mini-gap, AR processes are still observable at 500 mT.

Such sensitivity to time-reversal breaking indeed suggests that the observed mini-gap  $I_{excess}$  is due to the perfect AR of helical edge modes. Applying small magnetic fields destroys the perfect destructive interference of back-scattering paths,<sup>2</sup> opening the back-scattering channels in our structures. In this case, the probability of AR decreases, and  $I_{excess}$  vanishes.

In conclusion, we probe the recently discovered helical edge modes in InAs/GaSb QWs via Andreev reflection. Strong zero-bias dips in the differential resistance are observed as the Fermi level is tuned across the mini-gap. Evolution of the mini-gap differential resistance with applied bias as well as measured mini-gap excess current of  $\sim 150$  nA are in good agreement with the prediction of perfect Andreev reflection of the helical edge modes, necessitated by the absence of back-scattering channels. The perfect AR occurs in spite of a finite barrier at the interface and shows strong sensitivity to time-reversal breaking - hallmarks of helical nature of the QSH edges. Although sufficient coherence is not achieved in the junctions to observe a supercurrent, with further optimization in fabrication, InAs/GaSb readily arises as a viable platform where theoretical predictions of Majorana fermion modes<sup>11–13</sup> can be experimentally explored.

The work at Rice was supported by Rice Faculty Initiative Fund, Hackerman Advanced Research Program grant 003604-0062-2009, Welch Foundation grant C-1682, and NSF grant DMR-0706634. I.K. acknowl-

edges partial support from M. W. Keck Scholar. We thank D. C. Tsui for insightful discussions.

### Materials and Methods

The experiments are performed on high quality  $125\text{\AA}$  InAs/ $50\text{\AA}$  GaSb quantum wells in the inverted regime, patterned in a superconductor-normal metal-superconductor (S-N-S) junction geometry. Superconducting niobium electrodes with critical temperature of  $T_c = 8.27$  K are deposited directly on InAs layers via magnetron sputtering. Top layers of the contact region are selectively removed by etching, and plasma cleaned in argon atmosphere in-situ prior to niobium deposition.<sup>15–17</sup> The width and length of the junctions are  $W \sim 1 \mu\text{m}$  and  $L \sim 0.5 \mu\text{m}$ . The front gate is fabricated by depositing SiN using plasma enhanced chemical vapor deposition system, and evaporating a Ti/Au metal gate. Additional sample and processing details are given elsewhere.<sup>9,20</sup>

### Author contributions

I.K. fabricated the devices, performed the measurements, and analysed the data. G. S. prepared the sample wafer. R.R.D. supervised and provided continuous guidance for the experiments and analysis. Manuscript was prepared by I. K. and R. R. D.

The authors declare no competing financial interests.

- 
- <sup>1</sup> Hasan, M.Z. & Kane, C.L. Topological insulators. *Rev. Mod. Phys.* 82, 3045 (2010).
- <sup>2</sup> Qi, X.-L. & Zhang, S.C. Topological insulators and superconductors. *arXiv:1008.2026* (2010).
- <sup>3</sup> Fu, L., & Kane, C. L. Superconducting Proximity Effect and Majorana Fermions at the Surface of a Topological Insulator. *Phys. Rev. Lett.* 100, 096407, (2008).
- <sup>4</sup> Kane, C. L. & Mele, E. J. Quantum Spin Hall Effect in Graphene. *Phys. Rev. Lett.* 95, 226801 (2005).
- <sup>5</sup> Bernevig, B. A. & Zhang, S. C. Quantum Spin Hall Effect. *Phys. Rev. Lett.* 96, 106802 (2006).
- <sup>6</sup> Bernevig, B.A., Hughes, T.L. & Zhang, S. C. Quantum Spin Hall Effect and Topological Phase Transition in HgTe Quantum Wells. *Science* 314, 1757-1761 (2006).
- <sup>7</sup> Liu, C., Hughes, T.L., Qi, X.-L., Wang, K., & Zhang, S.-C. Quantum Spin Hall Effect in Inverted Type-II Semiconductors. *Phys. Rev. Lett.* 100, 236601 (2008).
- <sup>8</sup> Konig, M. et al. Quantum Spin Hall Insulator State in HgTe Quantum Wells. *Science* 318, 766-770 (2007).
- <sup>9</sup> Knez, I., Du, R.R., & Sullivan, G. Evidence for Helical Edge Modes in Inverted InAs/GaSb Quantum Wells. *arXiv:1105.0137* (2011).
- <sup>10</sup> Roth, A. et al. Nonlocal Transport in the Quantum Spin Hall State. *Science* 325, 294-297 (2009).
- <sup>11</sup> Nilsson, J., Akhmerov, A. R. & Beenakker, C. W. Splitting of a Cooper Pair by a Pair of Majorana Bound States. *Phys. Rev. Lett.* 101, 120403 (2008).
- <sup>12</sup> Fu, L. & Kane, C. L. Josephson current and noise at a superconductor/quantum-spin-Hall-insulator/superconductor junction. *Phys. Rev. B* 79, 161408 (2009).
- <sup>13</sup> Benjamin, C. & Pachos, J.K. Detecting Majorana bound states. *Phys. Rev. B* 81, 085101 (2010).
- <sup>14</sup> Adroguer, P. et al. Probing the helical edge states of a topological insulator by Cooper-pair injection. *Phys. Rev. B* 82, 081303(R) (2010).
- <sup>15</sup> Nguyen, C., Werking, J., Kroemer, H., & Hu, E.L. InAs-AlSb quantum well as superconducting weak link with high critical current density. *Appl. Phys. Lett.* 57, 87 (1990).
- <sup>16</sup> Heida, J. P., van Wees, B. J., Klapwijk, T. M. & Borghs, G. Critical currents in ballistic two-dimensional InAs-based superconducting weak links. *Phys. Rev. B* 60, 13135 (1990).
- <sup>17</sup> Giazotto, F. et al. Josephson Current in Nb/InAs/Nb Highly Transmissive Ballistic Junctions. *J. Sup.* 17, 317 (2004).
- <sup>18</sup> Naveh, Y. & Laikhtman, B. Band-structure tailoring by electric field in a weakly coupled electron-hole system. *Appl. Phys. Lett.* 66, 1980 (1995).
- <sup>19</sup> Yang, M. J., Yang, C. H., Bennett, B. R. & Shanabrook, B. V. Evidence of a Hybridization Gap in “Semimetallic” InAs/GaSb Systems. *Phys. Rev. Lett.* 78, 4613 (1997).
- <sup>20</sup> Knez, I., Du, R.R. & Sullivan, G. Finite conductivity in mesoscopic Hall bars of inverted InAs/GaSb quantum wells. *Phys. Rev. B* 81, 201301(R) (2010).
- <sup>21</sup> Andreev, A. F. Thermal conductivity of the intermediate state of superconductors. *Soviet. Phys. JETP* 19, 1228–1231 (1964).

- <sup>22</sup> Blonder, G. E., Tinkham, M. & Klapwijk, T. M. Transition from metallic to tunneling regimes in superconducting microconstrictions: Excess current, charge imbalance, and supercurrent conversion. *Phys. Rev. B* 25, 4515 (1982).
- <sup>23</sup> Octavio, M., Tinkham, M., Blonder, G. E. & Klapwijk, T. M. Subharmonic energy-gap structure in superconducting constrictions. *Phys. Rev. B* 27, 6739 (1983).
- <sup>24</sup> Flansberg, K., Bindslev Hansen, J. & Octavio, M. Subharmonic energy-gap structure in superconducting weak links. *Phys. Rev. B* 38, 8707 (1988).
- <sup>25</sup> Naveh, Y. & Laikhtman, B. Magnetotransport of coupled electron-holes. *Euro. Phys. Lett.* 55, 545 (2001).
- <sup>26</sup> Caldeira, A. & Legett, A. J. Influence of Dissipation on Quantum Tunneling in Macroscopic Systems. *Phys. Rev. Lett* 46, 211 (1981).
- <sup>27</sup> Recent experiments<sup>9</sup> show that low bulk conduction has little effect on edge conduction, presumably due to the large disparity in Fermi wave-vectors between bulk and edge states, allowing for simple addition of edge and bulk contributions.